Vol. 21, No. 3(2022) Ener2969
Revista Mexicana de Ingeniería Química

Esterification of oleic acid into biodiesel and use it as fuel in a diesel engine to determine its impact

Esterificación de ácido oleico para obtener biodiesel y utilizarlo como combustible en un motor a diésel para determinar su impacto

M. Sánchez-Cárdenas[1,2], L.A. Sánchez-Olmos[1,2*],F. Trejo-Zárraga[1], K. Sathish-Kumar[3]

[1]*CICATA-Legaria, Instituto Politecnico Nacional, Legaria 694, Col. Irrigacion, Del. Miguel Hidalgo, C.P. 11500, Ciudad de Mexico,Mexico.*
[2]*Dirección de Postgrado e Investigación, Universidad Politécnica de Aguascalientes, Calle Paseo San Gerardo 207, Aguascalientes, C.P. 20342, Ags, México.*
[3]*Instituto Tecnológico El Llano Aguascalientes (ITEL)/ Tecnológico Nacional de México (TecNM). Km 18 carr. Aguascalientes-San Luis Potosí, El Llano Ags., C.P. 20330, México.*

Received: September 30, 2022; Accepted: November 16, 2022

Abstract

In this study, experimentally obtained biodiesel was analyzed as an alternative source of energy from oleic acid, using pure methanol and a solid acid catalyst in an autogenous reactor, the main product obtained was biodiesel, achieving a yield of 96.72 percent and thus demonstrating a greater conversion of free fatty acids (FFA) to methyl esters, allowing them to be studied in a diesel engine. Sulfonation of vulcanized rubber carbon produced the solid acid catalyst. Three control variables were used in the engine for the realization and analysis of the biodiesel obtained vs. commercial diesel in the internal combustion engine. Pure commercial diesel (PDI), biodiesel-diesel blend (50/50)(MES), and pure biodiesel (BIOP). BIOP was able to produce less environmental contamination among the three samples. The combustion tests show that there is no significant variation using Box-Behnken method in the characteristics and performance of said tests; however, in the gaseous combustion products, significant reductions in carbon monoxide, unburned hydrocarbon, and an increase in greenhouse gas emissions were achieved. The greenhouse effect. nitrogen oxide when using the (PDI) versus the (MES). When MES and PBM were tested in a laboratory engine, the amount of NOx, CO, HC, and smoke emissions were reduced.
Keywords: Oleic acid, Mesoporous carbon, Biodiesel production, Solid acid catalyst, Sulfonation treatment.

Resumen

En este estudio se analizó el biodiesel obtenido experimentalmente como fuente alternativa de energía a partir del ácido oleico, utilizando metanol puro y un catalizador sólido ácido en un reactor autógeno, el principal producto obtenido fue el biodiesel, logrando un rendimiento del 96.72 por ciento y demostrando así un mayor conversión de ácidos grasos libres (FFA) a ésteres metílicos, lo que permite estudiarlos en un motor diesel. La sulfonación del carbón de llanta vulcanizada produjo el catalizador sólido ácido. Se utilizaron tres variables de control en el motor para la realización y análisis del biodiesel obtenido vs diesel comercial en el motor de combustión interna. Diésel comercial puro (PDI), mezcla biodiésel-diésel (50/50)(MES) y biodiésel puro (BIOP). BIOP pudo producir menos contaminación ambiental entre las tres muestras. Las pruebas de combustión muestran que no existe una variación significativa utilizando el método de Box-Behnken en las características y desempeño de dichas pruebas; sin embargo, en los productos de los gases de combustión se lograron reducciones significativas de monóxido de carbono, hidrocarburos no quemados y un aumento de las emisiones de gases de efecto invernadero. El efecto invernadero, óxido de nitrógeno cuando se utiliza el (PDI) frente al (MES). Cuando se probaron MES y PBM en un motor de laboratorio, se redujo la cantidad de emisiones de NOx, CO, HC y humo.
Palabras clave: Ácido oleico, Carbón mesoporoso, Producción de biodiésel, Catalizador solid ácido o, Tratamiento de sulfonación.

*Corresponding author. *E-mail*: luibandi_2000@hotmail.com
https://doi.org/10.24275/rmiq/Ener2969
ISSN:1665-2738, *issn-e*: 2395-8472

1 Introduction

Given the current state of environmental problems and the wide range of energy costs worldwide, some private companies, government agencies, and public and private research institutions are collaborating to develop new renewable energy alternatives to offset the use of fossil fuels (Beck *et al*., 2018; Dubey *et al*., 2021; Fangfang *et al*., 2021). To mitigate the environmental impact of energy, various technologies are being developed today to be used in the production of clean energy, resulting in greater efficiency and less environmental impact, and thus contributing to economic development (Badawy *et al*., 2021; Shboul *et al*., 2021; Sleiti *et al*., 2021). The usefulness of these engines in the diesel transport industry is growing due to their higher efficiency compared to gasoline engines, the fact that a diesel engine is more reliable, and, most importantly, the significant savings of biodiesel compared to other gasolines (Zhou *et al*., 2021; Al-Muhtaseb *et al*., 2021; Sheikholeslami *et al*., 2021). For these reasons, it is a global priority to develop alternative renewable biofuels that contribute to the reduction of pollutants emitted into the environment as a result of population growth and, as a result, increased fuel consumption (Temiz *et al*., 2021; Zul *et al*., 2021; Baskaran *et al*., 2021). Several countries around the world are currently updating the operation and construction standards of diesel engines, allowing them to comply with the standardized norms of atmospheric pollutants that are released into the environment during combustion (Pandey *et al*., 2021; Kanimozhi *et al*., 2021; Mahmood *et al*., 2021).

Significant progress has been made in the development of alternative biofuels in recent years, including biodiesel derived from vegetable oils and animal fats, among other products, which is regarded as a viable alternative to diesel due to its high oxygen content and renewable nature (Viswanathan *et al*., 2021; Leibensperger *et al*., 2021; Karami *et al*., 2022). On the other hand, industrial needs have led to the connection of their production processes with research centers to find new raw materials and, above all, economic for the production of biodiesel, as long as it does not interfere with the essential needs in supplies for human use, so the alternative raw materials are vegetable oils and animal fats, which are primarily used in human activities and then recycled for energy production (Moatamed *et al*., 2021; Thoppil *et al*., 2021; Dubey *et al*., 2022). Another option is to use oleic acid in the esterification reaction to produce methyl esters using various catalysts such as sodium hydroxide and potassium hydroxide, among others (Aparamarta *et al*., 2020; Al-Hatrooshi *et al*., 2020; AlKahlaway *et al*., 2021; Tokuyama *et al*., 2021). The heterogeneous acid carbonic catalyst is ideal for achieving mixture separation after the esterification process. Glycerin, biodiesel, and solid acid catalyst separation without the use of costly recovery processes (Malaika *et al*., 2021; Yuan *et al*., 2021; Yang *et al*., 2021; Alvear-Daza *et al*., 2021).

There are several methods for obtaining a solid acid catalyst; for this work, vulcanized rubber of a specific commercial brand was used, and the product was pyrolyzed. After obtaining the carbon, a sulfonation with 98.3 percent concentrated sulfuric acid was performed to achieve the placement of the acid sites in the mesoporous carbon. The use of an autogenous reactor reduces the reaction time for the production of methyl esters, lowering the production cost. In the current study, methanol was used as an alkylating agent in an autogenous intermittent semi-industrial type reactor, were used sulfonated solid carbon as an acid catalyst to produce pure biodiesel (MES). Later, we evaluate their efficiency inside the diesel engine, including the Pure commercial diesel (PDI)and biodiesel-diesel blend (50/50). It is important to note that no modifications were made to the diesel engine for the tests of power output and emissions of engine pollutants (NOx, CO, HC, and smoke.

2 Materials and methods

2.1 Material

The SIGMA-ALDRICH firm purchased pure oleic acid, reactive grade methyl alcohol, and 93.8 percent sulfuric acid for use as raw materials. Analytical reagent-grade chemicals were used throughout.

2.2 Catalyst preparation

8 g of uniformly crushed vulcanized rubber (7.5 × 1.0 mm and 1 mm thick pieces) were placed in a stainless steel microreactor to create the solid acid catalyst (CASOA) utilizing a thermally stable pyrolysis technique. Where it was heated to 500 ºC over two hours with an N2 flow of 30 ml/min and a prior heating ramp of 15 °C/min.

To sulfonate the carbonaceous material (MACA) produced by the pyrolysis reaction, 15 g of MACA and 250 ml of H_2SO_4 were combined and heated to 130 °C for 18 hours. The resulting sulfonated carbon was then filtered, washed with hot de-ionized water at 80 °C until a neutral pH was achieved, and finally placed in a muffle at 120 °C for 24 hours to remove residual water (Sánchez-Olmos *et al*., 2017; Zheng *et al*., 2021).

2.3 Catalyst characterization

The (CASOA) was subjected to various physical characterization methods, including Using an X-ray diffractometer of the Brucker model D8 type, and the crystallinity of carbonaceous materials was studied. Scanning electron microscopy (SEM), a JEOL JSM-6300-S electron microscope, and energy dispersion X-ray analysis (EDX) were utilized to produce high-resolution images of the surface of the (CASAO) via electron-matter interactions. On a Nicolet iS10 model spectrophotometer from Thermo Scientific, infrared spectroscopy (FTIR) was carried out. Using a Quantachrome Autosorb-1C piece of equipment, the nitrogen desorption method was used to measure the distribution of the pore size and surface area of the carbonaceous acid solid catalyst.

The total acidity and the resistance of the acid sites of the carbonaceous material were determined by thermally programmed desorption (TPD) of n-butylamine using an in-line Prisma model mass spectrometer. 0.2 g of sample, previously evacuated with He, was used for the adsorption/desorption studies in a quartz microreactor at atmospheric pressure and 0°C under a flow of He/Ar saturated with n-butylamine. The overall flow rate was 60 cm^3/min, and the n-butylamine partial pressure was 28.92 Torr. After that, the saturated sample was purged in neat He for 1 h to remove the remaining trapped n-butylamine, and then, the desorption of n-butylamine was recorded by heating at 10 °C/min (Sánchez-Olmos *et al*., 2020).

2.4 Esterification

To combine oleic acid (50 cm^3) and anhydrous methanol (132 cm^3) with the sulfonated carbon catalyst (0.045 percent w), the mixture was first agitated for 30 seconds before being added to the autogenous reactor (maximum capacity of 400 cm^3), and then the heating ramp (15 °C) was turned on to raise the temperature until it reached 225 °C with a reaction time of 23 minutes.

Table 2.1. Physicochemical properties and composition of Biodiesel.

Property	Unit	Biodiesel
Cloud point	°C	11.4
Could point	°C	6
Density al 15 °C	Kg/m^3	793.7
Flash point	°C	161
Heating Value	KJ/Kg	40
Kinematic Viscosity	mm^2/s, 40 °C	4.156
Pour point	°C	7.4

It is important to note that the operating conditions were maintained throughout the experiment to produce the highest-quality biodiesel (Salamon *et al*., 2020; Sánchez-Olmos *et al*., 2020).

The autogenous reactor starts to record the reaction time when it reaches 225 °C in temperature. The esterification reaction is reversible, thus at the end of the 23-minute reaction period, the reactor is immediately transferred to a cold water bath to terminate the reaction and prevent undesirable products. The reactor is unveiled and the byproducts are put in a decanting flask to rest as it cools Table 2.1. The excess unreacted methanol present was recovered by evaporation, and the sulfonated catalyst was collected by vacuum filtration. The catalyst and the glycerin produced were removed from the solution. A 1 cm^3 sample of the residual solution, which represented the methyl esters produced by the esterification reaction, was obtained and examined using a GC gas chromatograph to calculate the Biodiesel content. (Sánchez-Olmos *et al*., 2020; Chanthon *et al*., 2021).

2.5 Biofuel tests in a diesel engine

On a test bench with a diesel engine, the resulting biodiesel was examined for pollutant emissions, output power, the amount of NOx, CO, and HC, and the amount of smoke, all while considering the engine's speed. The experiments were conducted in a steady state at three speeds (1000 rpm, 1500 rpm, and 2200 rpm) for diesel.

On the test bench, pure commercial diesel (PDI), a blend of paraffinic, olefinic, and aromatic hydrocarbons produced during the refining of crude oil (PBM), and pure biodiesel (MES) were all employed, carried out in pairs.

2.6 Engine test

The injection temperature in the engine was normalized to 23 °C, 180 bar pressure, a compression ratio of 17.5:1, and a speed of 1500 RPM before starting the experimental portion on the test bench with the three types of fuel used. The diesel engine was fed with PDI for only 10 minutes to stabilize it. A computerized platform that displayed the predetermined operating parameters was then utilized to correct the engine continuously.

The aforementioned diesel engine was modified to fit a stationary dynamometer. The computer software "Engine Analysis Software" was used to record the test parameters with the proper fuel injection, temperatures, airflow, etc. for the mixtures used, and to determine the performance characteristics of the motor, thermal efficiency of the brake, rate of heat release, etc. The diesel engine and the dynamometer were discovered connected to a control panel and a computer. It is significant to note that the six experiments conducted in the diesel engine were done in duplicate and with high and low fuel loads for the PDI, PBM, and MES, respectively.

Additionally, an "AVL DITEST MDS 650" diesel engine exhaust gas examination was performed. The requirements are displayed in figure 3.9, and the "TESTO 338" smoke meter was used to measure the smoke opacity.

2.7 Analysis of uncertainty

By using a series of uncertainties-called perturbations, the parameters were computed. Airflow (1.1 percent), liquid fuel flow (0.1 percent), gas flow (2 percent), engine load (0.1 percent), engine speed (1.3 percent), cylinder pressure (0.8 percent), temperature (1.0 percent), and lower heating value (LCV) of liquid fuel are a few of the average uncertainties of the measured and calculated parameters (1.0 percent). Based on this, performance and engine combustion experiments have calculated accuracy within +/- 4.5 percent. The emission study's accuracy is only 4.5%, though. Brake Thermal Efficiency (BTE) and Brake Specific Fuel (BSFC) each have a maximum coefficient of variance value of 3 percent and 4 percent, respectively. While the maximum cylinder pressure, ignition delay, CO, HC, and NOx combustion emission measurements have revealed VOC of 5, 4, 2, 2, and 6% respectively.

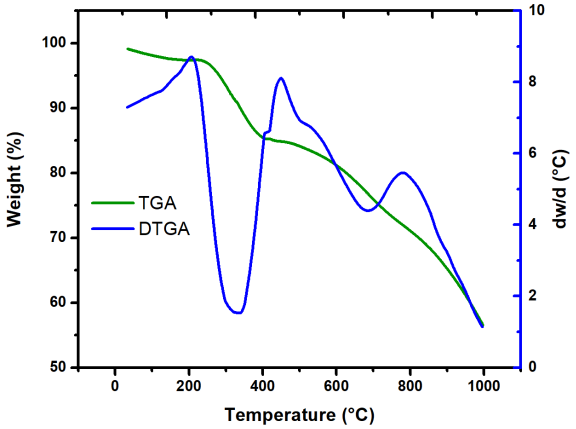

Figure 3.1. TGA and DTGA of the sulfonated carbon catalyst.

3 Results and discussion

3.1 Chemical and physical characterization of carbonaceous material

The elemental makeup of this material is closer to that of pyrolyzed carbon coke because the carbon utilized as the catalyst revealed a significant quantity of S in the carbonaceous structure of vulcanized rubber (Zhang *et al*., 2021). The number of acid sites in the catalyst that was obtained following the sulfonation treatment was counted using the acid-base titration method (Al-Mawali *et al*., 2021; Harisha *et al*., 2021). This catalyst's total acid density of 3.015 mmol/g indicates that its acid sites are very active. Because of this, CASOA was effectively employed to turn FFA-containing oleic acid into biodiesel. To test the thermal stability of the CASOA, thermogravimetry (TGA) was used in stable settings with a nitrogen flow as shown in figure 3.1.

It exhibits 4.6 percent mass loss by weight in the first transition zone between 35 and 318 degrees Celsius, which is attributed to the evaporation of water that was once inside the porous structure after washing and the groups of -OH that were inside the mesoporous structure. Since it is amorphous carbon, there is a second transition zone where the structure's remaining organic groups are observed to be losing strength, and the carbonaceous walls are deforming and collapsing. These events take place in the temperature range of 390 °C to 745 °C. It is also related to the removal of the carboxylic acid group (COOH) and other functional groups from the structure (Shi *et al*., 2021; Mekala

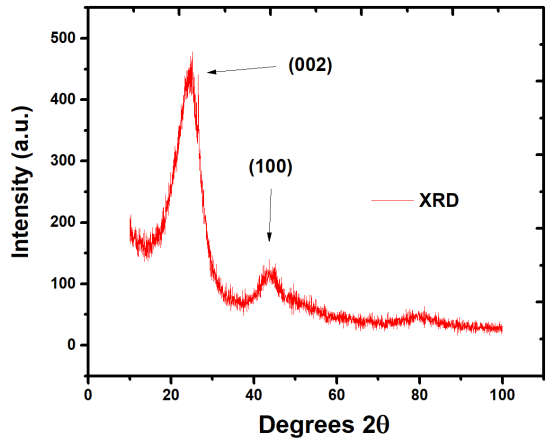

Figure 3.2. CASOA XRD patterns.

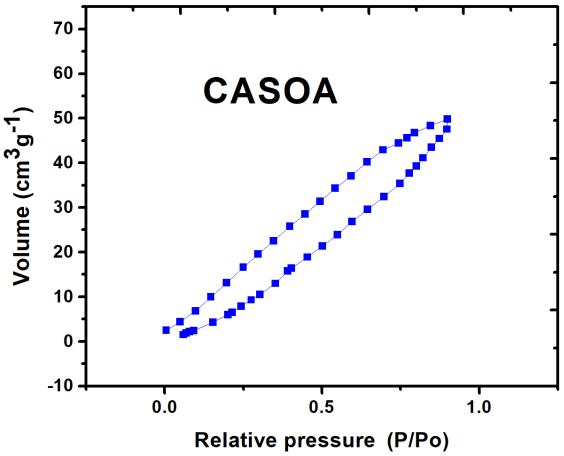

Figure 3.3. CASOA isotherm. N_2 adsorption.

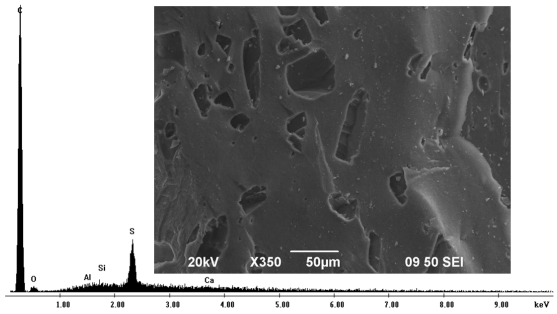

Fig. 3.4. SEM and EDX analysis of sulfonated carbon.

et al., 2022; Feng *et al*., 2022). Due to the existence and stability of the covalent link between the sulfonic acid site (-SOH) and the carbon surface, the whole disintegration of the material can be seen in the third zone of the analysis at high temperatures between 690 and 970 °C (Björk *et al*., 2021; Xie *et al*., 2021). Two distinctive peaks of CASOA are seen in the XRD examination of the sulfonated catalyst at 25° and 43.5°, as illustrated in figure 3.2. The nanolayer sheets found in the structure of the sulfonated catalyst are responsible for the 002 planes represented by the first peak. The material is categorized as an amorphous carbonaceous catalyst since it exhibits a second peak in plane 100 that represents the presence of a graphite structure in the catalyst (Zarnaghash *et al*., 2021; Thuppati *et al*., 2021).

The results of the BET analysis are presented in Table 3.1. When utilized as a catalyst, CASOA exhibits good surface area and porosity characteristics. A stable mesoporous structure was produced by the CASOA, which has a surface area of 99.5 m^2/g and is attributed to the direct sulfuric acid treatment of the carbonaceous structure. This process removed a significant portion of the impurities that were present during vulcanization but could not be removed during the pyrolysis process.

With a mesopore volume of 0.25 cm^3/g, the adsorption isotherm on the CASOA catalyst was type II. Using the IUPAC classification, which classifies pore diameters between 2 and 50 nm as mesoporous material and values 2 nm as micropores, two groups of mesopores were found in the sample during the examination. As seen in Figure 3.3, the majority of the pores present in the catalyst were 18.2 nm in size, but the CASOA only displayed a tiny number of pores with a dimension equivalent to 3.9 nm.

The SEM study performed on the CASOA catalyst revealed an uneven structure. The CASOA revealed that the catalyst is made up of agglomerations of irregular particles between 3 and 40 m in size. These agglomerations are the result of solid-state processes that sulfonate the carbonaceous structure (Chhabra *et al*., 2021; Chhetri *et al*., 2021). EDX analysis confirms the presence of a significant amount of S. The minimum emission voltage value of S (sulfur) was about 2.37 keV. According to this research, the amount of sulfur and carbon in the sulfonated catalyst increased (Fig. 3.4). 1.63 percent S was found in the sulfonated carbonaceous structure, and 3.91 percent S was found in the sulfonated carbon (an acid catalyst). This is explained by the fact that the mesoporous structure underwent a sulfonation process. Based on the rise in S that we observed, we can estimate that there are roughly 3 sulfur atoms and 6 oxygen atoms in the surface structure of the sulfonated catalyst for every 200 carbon atoms (Sánchez-Olmos *et al*., 2020; Hu *et al*., 2021).

Table 3.1. Textural parameters of the original and sulfonated carbons:

Sample	Specific surface, SBET (m^2/g)	Pore volume, VP (cm^3/g)	Pore average size, DP (nm)	Mesopore specific volume (cm^3/g)
CASOA	98.44	0.315	18.720	0.310

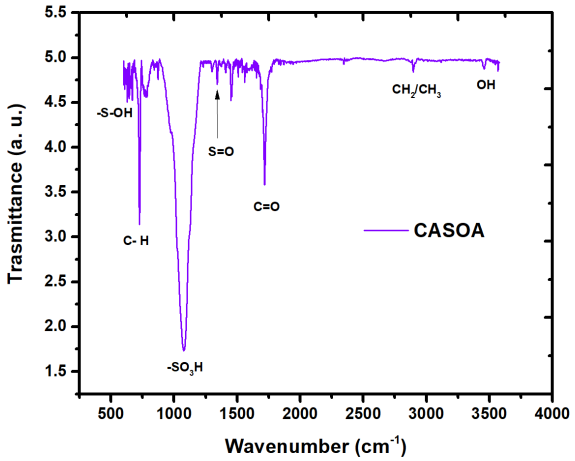

Fig. 3.5. FTIR spectra of sulfonated carbon.

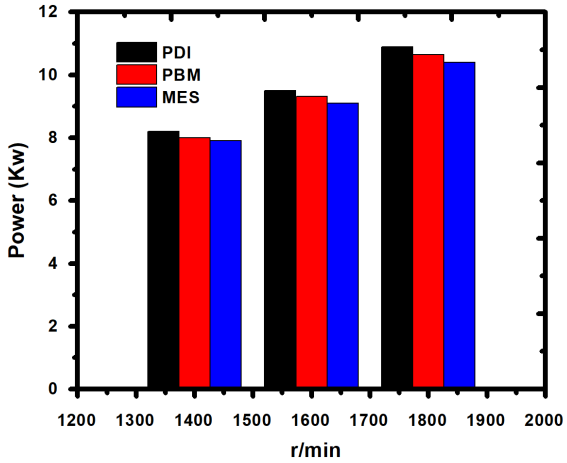

Fig. 3.6. Power output for PDI, PBM, and MES.

The CASOA's infrared spectroscopy investigation (Fig. 3.5.) reveals a weakly intense peak at 618 cm^{-1} that is associated with the S-O bond (Zhang *et al.*, 2021; Cao *et al.*, 2021). The C-H bond is represented by a second medium intensity peak at 727 cm^{-1}. The peak, which corresponds to the acid groups -SO_3H and symbolizes the symmetric vibration of O = S = O, is visible at 1075 cm^{-1} (Leesing *et al.*, 2021; Zhang *et al.*, 2021). The C-C aromatic bond is represented by a faint IR signal at 1255 cm^{-1}. The presence of the S=O bond is indicated by a peak at 1351 cm^{-1}, which is somewhat intense. The functional group C = C and the conjugated group C = O, respectively, have peaks at 1448 cm^{-1} and 1718 cm^{-1} with strong intensities (Zainol *et al.*, 2021; Zhu *et al.*, 2021). The low-intensity peak at 2910 cm^{-1} corresponds to the CH_2/CH_3 groups found in the carbonaceous structure.

The examination of the thermal desorption of n-butylamine on the surface of the CASOA catalyst allowed for the measurement of the acids that were present in its mesoporous structure, yielding the following acid values: CASOA equals 2.82 mmol g^{-1}. defines a large number of acid groups that are firmly anchored in the carbon shell of the sulfonated carbons (Fonseca *et al.*, 2020; Zailan *et al.*, 2021).

3.2 *Effects of reaction parameters*

The reaction parameters employed were a reflection of the efficiency of the process. primarily in how catalyst quantity (A), temperature (B), and reaction time interact (C). Contact between the oil and the methanol in the reaction mixture caused the catalyst to deactivate as a function of utilization in the reaction (Rodríguez-Ramírez *et al.*, 2020). The following parameters were applied to the Box-Behnken optimization model to produce the ideal reaction conditions: Catalyst concentration (A) = 0.045 percent by weight, reaction time (C) = 23 minutes, and temperature (B) = 225 °C, resulting in when all the factors are combined, a maximum equivalent yield of 96.72 percent biodiesel is produced. According to these statistical analyses, the model put forth by (Dwivedi *et al.*, 2015; Sánchez-Olmos *et al.*, 2019) is suitable for predicting the rate at which oleic acid turns into biodiesel in the context of the factors examined.

According to Sánchez-Olmos *et al.*, (2017); Liang *et al.*, 2021) Figure 3.6 depicts the behavior of biodiesel produced in a lab and its various mixtures, as well as that of petro-diesel in a diesel engine under ideal conditions. It also displays the power output for biodiesel (MES), a blend of commercial diesel and 50/50 biodiesel (PBM), and petro-diesel (PDI). There

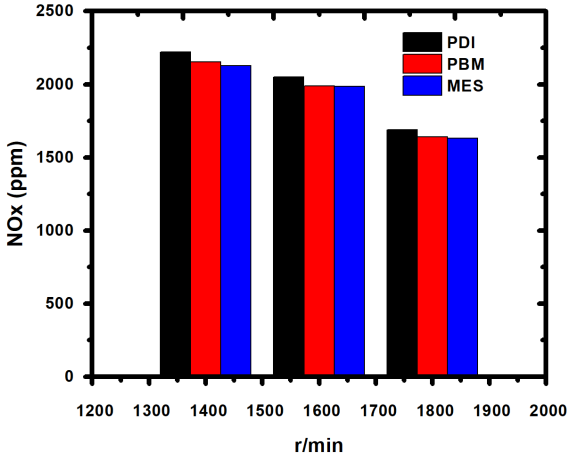

Fig. 3.7. NOx emission for PDI, PBM, and MES.

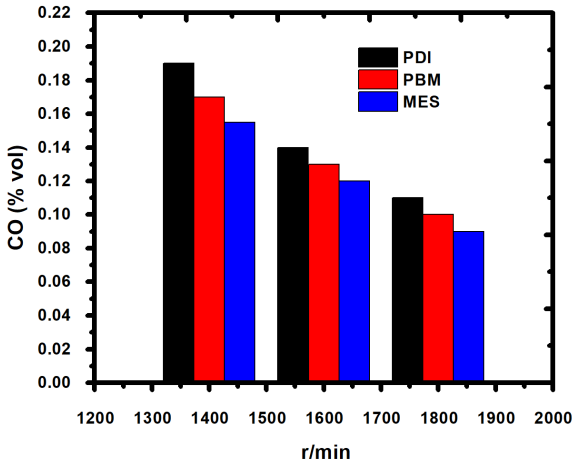

Fig. 3.8. CO emission for PDI, PBM, and MES.

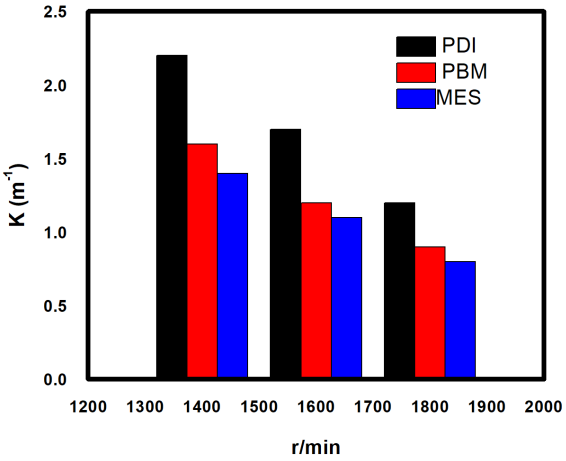

Fig. 3.9. Smoke emission for PDI, PBM, and MES.

was only a small amount of output power variation between PDI, PBM, and MES samples, about 1.9 percent. This decrease is a result of the calorific value of biodiesel (Avelino *et al*., 2021). Some authors published similar data when using biodiesel and diesel in an engine (Amid *et al*., 2021), where they mention a power reduction of four percent and attribute it to the calorific value of biodiesel. The oxygen included in the biodiesel molecule is also responsible for the decrease in power. In the engine, the PDI begins to cause combustion before the PBM and the MES. Due to their larger density and higher kinematic viscosity per methyl ester molecule, the PBM and MES samples' behaviors are attributed to a brief ignition delay as well as a delayed injection time (Subramanian *et al*., 2020).

When the adiabatic flame occurs, which relates to the temperature and atomization of the fuel inside the engine, the oxygen content in the methyl ester molecule is sensitive to NOx emissions at various speed ranges (Fig. 3.7) and varied fuel combinations (Ghanbari *et al*., 2021). The physical properties of fuel injection, the degree of mixing between the fuel and air inside the combustion chamber, the rate of evaporation, the geometry of the engine, and other factors can all affect how much NOx is produced by a diesel engine (Karpagarajan *et al*., 2021). The diesel engine's PBM and MES sample analysis revealed that NOx levels decreased as engine speed rose. This is explained by improved combustion chamber gas flow and volumetric efficiency (Akintunde *et al*., 2021). Similar to how MES and PBM react with a combination of air-containing nitrogen, their increased oxygen content compared to commercial diesel causes a higher production of NOx (Aisosa *et al*., 2021).

The levels of CO emissions from the PDI, PBM, and MES fuels may be seen in the emissions of the samples (Fig. 3.8). The amount of CO produced by burning reduced as engine speed rose. This is due to improved combustion, which is caused by the gasoline evaporating at the right temperature and pressure during injection into the engine cylinder, as well as a decline in the coefficient of surplus air (Jena *et al*., 2019). The gas mixture and cylinder temperature both have an impact on the engine's ability to produce CO (Khiraiya *et al*., 2021). Additionally, the oxygens are responsible for the decrease in the amount of CO created by combustion. The oxygen present in the biodiesel chains as a result of inadequate atomization is also responsible for the decrease in the quantity of CO produced during burning (Hosamani *et al*., 2021). Because combustion is improved at high temperatures in the cylinder, the PDI produced a larger CO emission

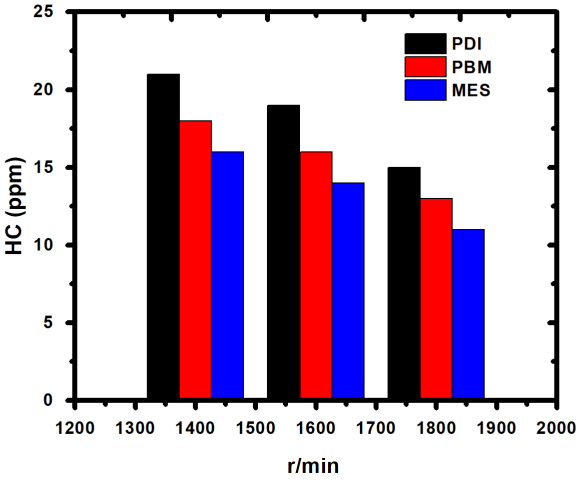

Fig. 3.10. HC emission for PDI, PBM, and MES.

than the samples that include biodiesel (Singh *et al*., 2021).

Lower values were seen in the samples containing biodiesel compared to PDI when the smog opacity (K) figure 3.9 was determined. K incurred a loss of value relative to the PDI of 32% in MES and a loss of value relative to the PDI of 23% in PBM. Due to the oxygen contained in the biodiesel molecule, which improves combustion and reduces soot production, the value of K with respect to the PDI has decreased (Gad *et al*., 2021).

Figure 3.10 depiction of the HC emissions tests. For the PDI, PBM, and MES samples, the decrease with increasing engine load can be seen. Using the MES as a benchmark, it had a lower HC emission compared to the PDI, and the PBM also showed a decline in HC value compared to the PDI. This is explained by the fact that the presence of the biodiesel molecule leads to better combustion because there is oxygen at the end of the chain (Geng *et al*., 2021). The presence of cetanes in the PBM and MES as a result of the delay produced while starting the diesel engine is another factor contributing to the reduction in HC emissions (Sánchez-Cárdenas *et al*., 2020; Sánchez-Cárdenas *et al*., 2020; Roy *et al*., 2021). Comparing the MES to the PDI, the average HC was found to have decreased by 24%. Figure 10 illustrates the difference in the HC levels in the PBM and PDI, which was an average reduction of 19%.

Conclusion

The esterification of oleic acid worked well with the CASOA material produced by the aforementioned production procedures. This demonstrates that vulcanized rubber carbon can be treated with sulfuric acid to remove contaminants both on the surface and within the carbon structure, which in turn helps to enhance the bonding of sulfonyl groups with strong acidic characteristics. It was simple to separate the heterogeneous catalyst from the liquid mixture and demonstrated good performance in the synthesis of biodiesel. The results showed that the esterification process had a maximum conversion rate of 96.72 percent.

The reaction conditions for this behavior were 225 °C reaction temperature, 23 min reaction time, and 0.045 percent catalyst by weight catalyst quantity. The results from the engine with PDI, PBM, and MES demonstrated the significance of kinematic viscosity and the relationship between biodiesel. Physical ignition is delayed with an increase in C18: 1, C18: 0, and C16: 0, as well as C16: 0, since a higher kinematic viscosity does not favor the combination of fuel and air, fuel evaporation, or combustion efficiency. Thus, the entire ignition timing is impacted by both physical and chemical ignition retardation. The highest HC and CO emissions were produced by PDI, which also had the lowest power indicated and the lowest NOx emissions. With BIOP, though, superior performance and emission characteristics were seen despite an increase in NOx emissions. Due to its lower caloric value and higher kinematic viscosity when compared to Commercial Diesel-PDI (100%), and Mixed-MES (50-50%) performed marginally worse in terms of its properties. In comparison to PDI, CO and HC emissions rise by 5% at low loads, but fall by roughly 30% at medium and high loads, while there is a 5% rise in emissions at low loads. However, NOx emissions are reduced by around 30% for medium and high loads. Biodiesel's oxygen content is advantageous and enhances in-cylinder combustion at high loads.

References

Aisosa Oni, B., Eshorame Sanni, S., Daramola, M., Victoria Olawepo, A. (2021). Effects of oxy-acetylation on performance, combustion

and emission characteristics of *Botryococcus braunii* microalgae biodiesel-fuelled CI Engines. *Fuel 296*, 120675. https://doi.org/10.1016/j.fuel.2021.120675

Akintunde, S.B., Obayopo, S.O., Adekunle, A.S., Obisesan, O.R., Olaoye, O.S. (2021). Combustion and emission study of sandbox seed oil biodiesel performance in a compression ignition (CI) engine. *Energy Reports 7*, 3869-3876. https://doi.org/10.1016/j.egyr.2021.06.070

Al Hatrooshi, A.S., Eze, V.C., Harvey, A.P. (2020). Production of biodiesel from waste shark liver oil for biofuel applications. *Renewable Energy 145*, 99-105. https://doi.org/10.1016/j.renene.2019.06.002

AlKahlaway, A.A., Betiha, M.A., Aman, D., Rabie, A.M. (2021). Facial synthesis of ferric molybdate ($Fe_2(MoO_4)_3$) nanoparticle and its efficiency for biodiesel synthesis via oleic acid esterification. *Environmental Technology and Innovation 22*, 101386. https://doi.org/10.1016/j.eti.2021.101386

Al-Mawali, K.S., Osman, A.I., Al-Muhtaseb, A.H., Mehta, N., Jamil, F., Mjalli, F., Vakili-Nezhaad, G.R., Rooney, D.W. (2021). Life cycle assessment of biodiesel production utilising waste date seed oil and a novel magnetic catalyst: A circular bioeconomy approach. *Reneweable Energy 170*, 832-846. https://doi.org/10.1016/j.renene.2021.02.027

Al-Muhtaseb, A.H., Osman, A.I., Murphin Kumar, P.S., Jamil, F., Al-Haj, L., Al Nabhani, A., Kyaw, H.H., Myint, M.T.Z., Mehta, N., Rooney, D.W. (2021). Circular economy approach of enhanced bifunctional catalytic system of CaO/CeO_2 for biodiesel production from waste loquat seed oil with life cycle assessment study. *Energy Conversion and Management 236*, 114040. https://doi.org/10.1016/j.enconman.2021.114040

Alvear-Daza, J.J., Pasquale, G.A., Rengifo-Herrera, J.A., Romanelli, G.P., Pizzio, L.R. (2021). Mesoporous activated carbon from sunflower shells modified with sulfonic acid groups as solid acid catalyst for itaconic acid esterification. *Catalysis Today 372*, 51-58. https://doi.org/10.1016/j.cattod.2020.12.011

Amid, S., Aghbashlo, M., Peng, W., Hajiahmad, A., Najafi, B., Ghaziaskar, H.S., Rastegari, H., Mohammadi, P., Hosseinzadeh-Bandbafha, H., Lam, S.S., Tabatabaei, M. (2021). Exergetic performance evaluation of a diesel engine powered by diesel/biodiesel mixtures containing oxygenated additive ethylene glycol diacetate. *Science of the Total Environment. 792*. https://doi.org/10.1016/j.scitotenv.2021.148435

Aparamarta, H.W., Gunawan, S., Husin, H., Azhar, B., Tri Aditya, H. (2020). The effect of high oleic and linoleic fatty acid composition for quality and economical of biodiesel from crude Calophyllum inophyllum oil (CCIO) with microwave-assisted extraction (MAE), batchwise solvent extraction (BSE), and combination of MAE-BSE methods. *Energy Reports 6*, 3240-3248. https://doi.org/10.1016/j.egyr.2020.11.197

Avelino, A.F.T., Lamers, P., Zhang, Y., Chum, H. (2021). Creating a harmonized time series of environmentally-extended input-output tables to assess the evolution of the US bioeconomy - A retrospective analysis of corn ethanol and soybean biodiesel. *Journal of Cleaner Production 321*, 128890. https://doi.org/10.1016/j.jclepro.2021.128890

Badawy, T., Mansour, M.S., Daabo, A.M., Abdel Aziz, M.M., Othman, A.A., Barsoum, F., Basouni, M., Hussien, M., Ghareeb, M., Hamza, M., Wang, C., Wang, Z., Fadhil, A.B. (2021). Selection of second-generation crop for biodiesel extraction and testing its impact with nano additives on diesel engine performance and emissions. *Energy 237*. https://doi.org/10.1016/j.energy.2021.121605

Baskaran, V., Saravanane, R. (2021). Rendering utility water with solar still and efficiency of solar stills with different geometry - A review. *Environmental Nanotechnology, Monitoring and Management 16*, 100534. https://doi.org/10.1016/j.enmm.2021.100534

Beck, H.E., Zimmermann, N.E., McVicar, T.R., Vergopolan, N., Berg, A., Wood, E.F. (2018). Present and future köppen-geiger climate classification maps at 1-km resolution. *Scientific Data 5*, 1-12. https://doi.org/10.1038/sdata.2018.214

Björk, E.M., Atakan, A., Wu, P.H., Bari, A., Pontremoli, C., Zheng, K., Giasafaki, D., Iviglia, G., Torre, E., Cassinelli, C., Morra, M., Steriotis, T., Charalambopoulou, G., Boccaccini, A.R., Fiorilli, S., Vitale-Brovarone, C., Robertsson, F., Odén, M. (2021). A shelf-life study of silica- and carbon-based mesoporous materials. *Journal of Industrial & Engineering Chemistry 101*, 205-213. https://doi.org/10.1016/j.jiec.2021.06.011

Cao, M., Peng, L., Xie, Q., Xing, K., Lu, M., Ji, J. (2021). Sulfonated Sargassum horneri carbon as solid acid catalyst to produce biodiesel via esterification. *Bioresources Technology 324*, 124614. https://doi.org/10.1016/j.biortech.2020.124614

Chanthon, N., Ngaosuwan, K., Kiatkittipong, W., Wongsawaeng, D., Appamana, W., Quitain, A.T., Assabumrungrat, S. (2021). High-efficiency biodiesel production using rotating tube reactor: New insight of operating parameters on hydrodynamic regime and biodiesel yield. *Renewable and Sustainable Energy Reviews 151*, 111430. https://doi.org/10.1016/j.rser.2021.111430

Chhabra, T., Dhingra, S., Nagaraja, C.M., Krishnan, V. (2021). Influence of Lewis and Brønsted acidic sites on graphitic carbon nitride catalyst for aqueous phase conversion of biomass derived monosaccharides to 5-hydroxymethylfurfural. *Carbon N. Y. 183*, 984-998. https://doi.org/10.1016/j.carbon.2021.07.076

Chhetri, K., Dahal, B., Mukhiya, T., Tiwari, A.P., Muthurasu, A., Kim, T., Kim, H., Kim, H.Y. (2021). Integrated hybrid of graphitic carbon-encapsulated CuxO on multilayered mesoporous carbon from copper MOFs and polyaniline for asymmetric supercapacitor and oxygen reduction reactions. *Carbon N. Y. 179*, 89-99. https://doi.org/10.1016/j.carbon.2021.04.028

Dubey, A., Prasad, R.S., Kumar Singh, J., Nayyar, A. (2022). Optimization of diesel engine performance and emissions with biodiesel-diesel blends and EGR using response surface methodology (RSM). *Cleaner Engineering Technology 8*, 100136. https://doi.org/10.1016/j.clet.2022.100509

Dubey, S., Sharma, A., Panchariya, V.K., Goyal, M.K., Surampalli, R.Y., Zhang, T.C. (2021). Regional sustainable development of renewable natural resources using Net Primary Productivity on a global scale. *Ecological Indicators 127*, 107768. https://doi.org/10.1016/j.ecolind.2021.107768

Dwivedi, G., Sharma, M.P. (2015). Erratum: Application of Box-Behnken design in optimization of biodiesel yield from Pongamia oil and its stability analysis. *Fuel (2015) 145* (256-262) DOI: 10.1016/j.fuel.2014.12.063.

Fangfang, F., Alagumalai, A., Mahian, O. (2021). Sustainable biodiesel production from waste cooking oil: ANN modeling and environmental factor assessment. *Sustainable Energy and Technology Assessments 46*, 101265. https://doi.org/10.1016/j.seta.2021.101265

Feng, Y.Y., Chen, Y.Q., Wang, Z., Wei, J. (2022). Synthesis of mesoporous carbon materials from renewable plant polyphenols for environmental and energy applications. Xinxing Tan Cailiao/*New Carbon Materials 37*, 196-222. https://doi.org/10.1016/S1872-5805(22)60577-8

Fonseca, J.M., Spessato, L., Cazetta, A.L., Bedin, K.C., Melo, S.A.R., Souza, F.L., Almeida, V.C. (2020). Optimization of sulfonation process for the development of carbon-based catalyst from crambe meal via response surface methodology. *Energy Conversion Management 217*, 112975. https://doi.org/10.1016/j.enconman.2020.112975

Gad, M.S., Ismail, M.A. (2021). Effect of waste cooking oil biodiesel blending with gasoline and kerosene on diesel engine performance, emissions and combustion characteristics. *Process Safety and Environmental Protection 149*, 1-10. https://doi.org/10.1016/j.psep.2020.10.040

Geng, L., Bi, L., Li, Q., Chen, H., Xie, Y. (2021). Experimental study on spray characteristics, combustion stability, and emission performance of a CRDI diesel engine operated with biodiesel-ethanol blends. *Energy Reports 7*, 904-915. https://doi.org/10.1016/j.egyr.2021.01.043

Ghanbari, M., Mozafari-Vanani, L., Dehghani-Soufi, M., Jahanbakhshi, A. (2021). Effect of alumina nanoparticles as additive with diesel-biodiesel blends on performance and emission characteristic of a six-cylinder diesel engine using response surface methodology (RSM). *Energy Conversion and Management X 11*, 100091. https://doi.org/10.1016/j.ecmx.2021.100091

Harisha, P., Anil Kumar, B.N., Tilak, S.R., Ganesh, C. (2021). Production and optimization of biodiesel from composite Pongamia oil, animal fat oil and waste cooking oil using RSM. *Materials Today Proceedings 47*, 4901-4905. https://doi.org/10.1016/j.matpr.2021.06.322

Hosamani, B.R., Abbas Ali, S., Katti, V. (2021). Assessment of performance and exhaust emission quality of different compression ratio engine using two biodiesel mixture: Artificial neural network approach. Alexandria Eng. J. 60, 837-844. https://doi.org/10.1016/j.aej.2020.10.012

Hu, T., Yang, D., Gao, H., Li, Y., Liu, x., xu, K., Xa, Q., Ma, F. (2021). Atomic structure and electronic properties of the intercalated Pb atoms underneath a graphene layer. *Carbon N. Y. 179*, 151-158. https://doi.org/10.1016/j.carbon.2021.04.020

Jena, S.P., Mahapatra, S., Acharya, S.K. (2019). Optimization of performance and emission characteristics of a diesel engine fueled with Karanja biodiesel using Grey-Taguchi method. *Materials Today Proceedings 41*, 180-185. https://doi.org/10.1016/j.matpr.2020.08.579

Kanimozhi, B., kumar, G., Alsehli, M., Elfasakhany, A., Veeman, D., Balaji, S., thiran, T., Praveen Kumar, T.R., Sekar, M. (2021). Effects of oxyhydrogen on the CI engine fueled with the biodiesel blends: A performance, combustion and emission characteristics study. *International Journal of Hydrogen Energy*. https://doi.org/10.1016/j.ijhydene.2021.08.054

Karami, R., Hoseinpour, M., Hassan, N.M.S., Rasul, M.G., Khan, M.M.K. (2022). Exergy, Energy, and Emissions Analyses of Binary and Ternary Blends of Seed Waste Biodiesel of Tomato, Papaya, and Apricot in a Diesel Engine. *Energy Conversion and Management X 16*, 100288. https://doi.org/10.1016/j.ecmx.2022.100288

Karpagarajan, S., Jayakumar, T., Anandhan, R., Kannan, P., Neducheralathan, E., Arunprasad, J. (2021). Experimental investigation of performance and emission characterstics of jatropha biodiesel with Ruthenium oxide. *Materials Today Proceeding*. https://doi.org/10.1016/j.matpr.2021.03.472

Khiraiya, K., Ramana, P. V., Panchal, H., Sadasivuni, K.K., Doranehgard, M.H., Khalid, M. (2021). Diesel-fired boiler performance and emissions measurements using a combination of diesel and palm biodiesel. *Case Studies in Thermal Engineering 27*, 101324. https://doi.org/10.1016/j.csite.2021.101324

Leesing, R., Siwina, S., Fiala, K. (2021). Yeast-based biodiesel production using sulfonated carbon-based solid acid catalyst by an integrated biorefinery of durian peel waste. *Renewable Energy 171*, 647-657. https://doi.org/10.1016/j.renene.2021.02.146

Leibensperger, C., Yang, P., Zhao, Q., Wei, S., Cai, X. (2021). The synergy between stakeholders for cellulosic biofuel development: Perspectives, opportunities, and barriers. *Renewable and Sustainable Energy Reviews 137*, 110613. https://doi.org/10.1016/j.rser.2020.110613

Liang, M.S. (2021). Assessing emission and power tradeoffs of biodiesel and n-Butanol in diesel blends for fuel sustainability. *Fuel 283*, 118861. https://doi.org/10.1016/j.fuel.2020.118861

Mahmood, F., Bicer, Y., Al-Ansari, T. (2021). Design and thermodynamic assessment of a solar powered energy-food-water nexus driven multigeneration system. *Energy Reports 7*, 3033-3049. https://doi.org/10.1016/j.egyr.2021.05.032

Malaika, A., Ptaszyńska, K., Morawa Eblagon, K., Pereira, M.F.R., Figueiredo, J.L., Kozłowski, M. (2021). Solid acid carbon catalysts for sustainable production of biofuel enhancers via transesterification of glycerol with ethyl

acetate. *Fuel 304*. https://doi.org/10.1016/j.fuel.2021.121381

Mekala, S.P., Prabu, M., Gawali, S.D., Gopakumar, K., Gogoi, P., Bhatkar, A.R., Mohapatra, G., Unnikrishanan, E., Raja, T. (2022). Green synthesis of cyclohexanone to adipic acid over Fe-W oxides incorporated mesoporous carbon support. *Catalysis Communications 168*, 106466. https://doi.org/10.1016/j.catcom.2022.106466

Moatamed Sabzevar, A., Ghahramaninezhad, M., Niknam Shahrak, M. (2021). Enhanced biodiesel production from oleic acid using TiO_2-decorated magnetic ZIF-8 nanocomposite catalyst and its utilization for used frying oil conversion to valuable product. *Fuel 288*, 119586. https://doi.org/10.1016/j.fuel.2020.119586

Pandey, A.K., Ali Laghari, I., Reji Kumar, R., Chopra, K., Samykano, M., Abusorrah, A.M., Sharma, K., Tyagi, V. V. (2021). Energy, exergy, exergoeconomic and enviroeconomic (4-E) assessment of solar water heater with/without phase change material for building and other applications: A comprehensive review. *Sustainable Energy Technology Assessments 45*, 101139. https://doi.org/10.1016/j.seta.2021.101139

Rodríguez-Ramírez, R., Romero-Ibarra, I., Vazquez-Arenas, J. (2020). Synthesis of sodium zincsilicate (Na_2ZnSiO_4) and heterogeneous catalysis towards biodiesel production via Box-Behnken design. *Fuel 280*, 118668. https://doi.org/10.1016/j.fuel.2020.118668

Roy, A., Dabhi, Y., Brahmbhatt, H., Chourasia, S.K. (2021). Effect of emulsified fuel based on dual blend of Castor-Jatropha biodiesel on CI engine performance and emissions. *Alexandria Engineering Journal 60*, 1981-1990. https://doi.org/10.1016/j.aej.2020.12.003

Salamon, E., Cornejo, I., Mmbaga, J.P., Kołodziej, A., Lojewska, J., Hayes, R.E. (2020). Investigations of a three channel autogenous reactor for lean methane combustion. *Chemical Engineering Processing - Process Intensification 153*. https://doi.org/10.1016/j.cep.2020.107956

Sánchez-Cárdenas, M., Sánchez-Olmos, L. A., Sathish-Kumar, K., Trejo-Zarraga, F., Maldonado-Ruelas, V. A., & Ortiz-Medina, R. A. (2020). Controlled Evaluation in a Diesel Engine of the Biofuel Obtained with Ni/γ-Al_2O_3 Nanoparticles in the Hydrodeoxygenation of Oleic Acid. *International Journal of Chemical Reactor Engineering*. doi: 10.1515/ijcre-2019-0136

Sánchez-Cárdenas, M., Sánchez-Olmos, L.A., Sathish-Kumar, K., Trejo-Zarraga, F., Rodríguez-Valadez, F.J. (2021). Evaluation of the performance and atmospheric emissions in a diesel engine of the biofuel obtained by hydrodeoxygenation of oleic acid with Pt/γ-Al_2O_3 catalysts. *Environmental Progress & Sustainable Energy*, 1-9. https://doi.org/10.1002/ep.13582

Sánchez-Olmos, L.A., Medina-Valtierra, J., Sathish-Kumar, K., Sánchez Cardenas, M. (2017). Sulfonated char from waste tire rubber used as strong acid catalyst for biodiesel production. *Environmental Progress and Sustainable Energy*. https://doi.org/10.1002/ep.12499

Sánchez-Olmos, L.A., Sánchez-Cárdenas, M., Sathish-Kumar, K., Tirado-González, D.N., Maldonado-Ruelas, V.A., Ortiz-Medina, R.A. (2019). Effect of the sulfonated catalyst in obtaining biodiesel when used in a diesel engine with controlled tests. *Revista Mexicana de Ingeniería Química*. https://doi.org/10.24275/rmiq/ie831

Sánchez-Olmos, L.A., Sánchez-Cárdenas, M., Sathish-Kumar, K., Tirado-González, D.N., Rodríguez-Valadez, F.J. (2020). Sulfonated rim rubber used as a solid catalyst for the biodiesel production with oleic acid and optimized by Box-Behnken method. *Revista Mexicana de Ingeniería Química*. https://doi.org/10.24275/rmiq/Cat1625

Shboul, B., AL-Arfi, I., Michailos, S., Ingham, D., AL-Zoubi, O.H., Ma, L., Hughes, K., Pourkashanian, M. (2021). Design and Techno-economic assessment of a new hybrid system of a solar dish Stirling engine integrated with a horizontal axis wind turbine for microgrid power generation. *Energy Conversion*

Management 245, 114587. https://doi.org/10.1016/j.enconman.2021.114587

Sheikholeslami, M., Farshad, S.A. (2021). Investigation of solar collector system with turbulator considering hybrid nanoparticles. *Renewable Energy 171*, 1128-1158. https://doi.org/10.1016/j.renene.2021.02.137

Shi, Y., Hou, Y., Wang, Y., Zhang, J.J., Wang, H., Lu, J. X. (2021). Ordered mesoporous carbon loaded with $NiCO_2O_4$ as an electrocatalyst for electrocarboxylation of benzophenone. *Microporous and Mesoporous Materials 323*, 111174. https://doi.org/10.1016/j.micromeso.2021.111174

Singh, A., Sinha, S., Choudhary, A.K., Sharma, D., Panchal, H., Sadasivuni, K.K. (2021). An experimental investigation of emission performance of heterogenous catalyst jatropha biodiesel using RSM. *Case Studies in Thermal Engineering 25*. https://doi.org/10.1016/j.csite.2021.100876

Sleiti, A.K., Al-Ammari, W.A., Al-Khawaja, M. (2021). Integrated novel solar distillation and solar single-effect absorption systems. *Desalination 507*, 115032. https://doi.org/10.1016/j.desal.2021.115032

Subramanian, K., Sathiyagnanam, A.P., Damodharan, D., Sivashanmugam, N. (2020). Artificial Neural Network based prediction of a direct injected diesel engine performance and emission characteristics powered with biodiesel. *Materials Today Proceedings 43*, 1049-1056. https://doi.org/10.1016/j.matpr.2020.08.015

Temiz, M., Dincer, I. (2021). Concentrated solar driven thermochemical hydrogen production plant with thermal energy storage and geothermal systems. *Energy 219*, 119554. https://doi.org/10.1016/j.energy.2020.119554

Thoppil, Y., Zein, S.H. (2021). Techno-economic analysis and feasibility of industrial-scale biodiesel production from spent coffee grounds. *Journal of Clean Products 307*, 127113. https://doi.org/10.1016/j.jclepro.2021.127113

Thuppati, U.R., Choi, C., Machida, H., Norinaga, K. (2021). A comprehensive study on butanolysis of furfuryl alcohol to butyl levulinate using tungstated zirconia and sulfonated carbon catalysts. *Carbon Resources Conversion 4*, 111-121. https://doi.org/10.1016/j.crcon.2021.03.003

Tokuyama, H., Ohno, H., Fujita, T. (2021). Effect of polymer matrices of gels bearing a sulfo group on their catalytic properties for acetalization of glycerol to solketal and esterification of oleic acid to ethyl oleate. *Reactive Functions Polymers 165*, 104943. https://doi.org/10.1016/j.reactfunctpolym.2021.104943

Viswanathan, K., Wang, S., Esakkimuthu, S. (2021). Impact of yttria stabilized zirconia coating on diesel engine performance and emission characteristics fuelled by lemon grass oil biofuel. *Journal of Thermal and Analytical Calorimetry 146*, 2303-2315. https://doi.org/10.1007/s10973-020-10364-z

Xie, Y., Zhang, Z., Dong, Z., Zhou, R., Cao, X., Liu, Y., Hu, B., Yang, H., Wang, X. (2021). Functionalized mesoporous carbon nanospheres for efficient uranium extraction from aqueous solutions. *Environmental Nanotechnology, Monitoring Management 16*, 100510. https://doi.org/10.1016/j.enmm.2021.100510

Yang, H., Joh, H.I., Choo, H., Choi, Jae wook, Suh, D.J., Lee, U., Choi, Jungkyu, Ha, J.M. (2021). Condensation of furans for the production of diesel precursors: A study on the effects of surface acid sites of sulfonated carbon catalysts. *Catalysis Today 375*, 155-163. https://doi.org/10.1016/j.cattod.2020.05.006

Yuan, C., Wang, X., Yang, X., Alghamdi, A.A., Alharthi, F.A., Cheng, X., Deng, Y. (2021). Sulfonic acid-functionalized core-shell Fe_3O_4@carbon microspheres as magnetically recyclable solid acid catalysts. *Chinese Chemical Letters 32*, 2079-2085. https://doi.org/10.1016/j.cclet.2020.11.027

Zailan, Z., Tahir, M., Jusoh, M., Zakaria, Z.Y. (2021). A review of sulfonic group bearing porous carbon catalyst for biodiesel production. *Renewable Energy 175*, 430-452. https://doi.org/10.1016/j.renene.2021.05.030

Zainol, M.M., Asmadi, M., Iskandar, P., Wan Ahmad, W.A.N., Amin, N.A.S., Hoe, T.T. (2021). Ethyl levulinate synthesis from biomass derivative chemicals using iron doped sulfonated carbon cryogel catalyst. *Journal of Cleaner Production 281*, 124686. https://doi.org/10.1016/j.jclepro.2020.124686

Zarnaghash, N., Rezaei, R., Hayati, P., Moaser, A.G., Doroodmand, M.M. (2021). Shape-controlled synthesis of sodium zincate mesoporous structures based on sulfonated melamine formaldehyde and their application as catalysts for Biginelli reaction. *Journal of Molecular Structure 1232*. https://doi.org/10.1016/j.molstruc.2021.130028

Zhang, B., Gao, M., Geng, J., Cheng, Y., Wang, X., Wu, C., Wang, Q., Liu, S., Cheung, S.M. (2021). Catalytic performance and deactivation mechanism of a one-step sulfonated carbon-based solid-acid catalyst in an esterification reaction. *Renewable Energy 164*, 824-832. https://doi.org/10.1016/j.renene.2020.09.076

Zhang, J., Chen, S., Li, J., Han, W., Sun, X., Li, N., Hu, Z., Wang, L. (2021). Sulfonated carbon nano-onion incorporated polyethersulfone nanocomposite ultrafiltration membranes with improved permeability and antifouling property. *Separation and Purification Technology 256*. https://doi.org/10.1016/j.seppur.2020.117825

Zhang, P., Zhang, J., Sun, Z., He, C., Pan, B., Xing, B. (2021). The conductivity and redox properties of pyrolyzed carbon mediate methanogenesis in paddy soils with ethanol as substrate. *Scientific Total Environment 795*, 148906. https://doi.org/10.1016/j.scitotenv.2021.148906

Zheng, Q., Kato, T., Ito, Y., Wagatsuma, M., Hiraga, Y., Watanabe, M. (2021). Sulfonated carbon-catalyzed deamination of alanine under hydrothermal conditions. *Journal of Supercritical Fluids 175*, 105275. https://doi.org/10.1016/j.supflu.2021.105275

Zhou, X., Wu, L., Xiao, G., Tong, Z., Li, H. (2021). Experimental investigation and economic analysis on a solar pure water and hot water hybrid system. *Applied Thermal Engineering 195*, 117182. https://doi.org/10.1016/j.applthermaleng.2021.117182

Zhu, Y., Xu, T., Zhao, D., Li, F., Liu, W., Wang, B., An, B. (2021). Adsorption and solid-phase photocatalytic degradation of perfluorooctane sulfonate in water using gallium-doped carbon-modified titanate nanotubes. *Chemical Engineering Journal. 421*, 129676. https://doi.org/10.1016/j.cej.2021.129676

Zul, N.A., Ganesan, S., Hamidon, T.S., Oh, W. Da, Hussin, M.H. (2021). A review on the utilization of calcium oxide as a base catalyst in biodiesel production. *Journal of Environmental Chemical Engineering 9*, 105741. https://doi.org/10.1016/j.jece.2021.105741